SCIENCE CHINA
Information Sciences

• RESEARCH PAPER •

February 2024, Vol. 67, Iss. 2, 122404:1–122404:11
https://doi.org/10.1007/s11432-023-3745-y

Investigation and mitigation of Mott neuronal oscillation fluctuation in spiking neural network

Lindong WU[1†], Zongwei WANG[1,2*†], Lin BAO[1,3], Linbo SHAN[1], Zhizhen YU[1], Yunfan YANG[1], Shuangjie ZHANG[1], Guandong BAI[4], Cuimei WANG[1,2], John ROBERTSON[4], Yuan WANG[1,2], Yimao CAI[1,2*] & Ru HUANG[1,2]

[1]*School of Integrated Circuits, Peking University, Beijing* 100871*, China;*
[2]*Beijing Advanced Innovation Center for Integrated Circuits, Beijing* 100871*, China;*
[3]*State Key Laboratory of Information Photonics and Optical Communications, Beijing University of Posts and Telecommunications, Beijing* 100871*, China;*
[4]*Department of Engineering, University of Cambridge, Cambridge* CB2 1PZ*, UK*

Received 6 January 2023/Revised 9 March 2023/Accepted 18 April 2023/Published online 22 January 2024

Abstract Mott devices, featuring low hardware cost and high energy efficiency, have been demonstrated as a key oscillatory element in artificial neurons to enable spiking neural networks (SNNs) such as conversion-based SNNs (CSNNs). However, there will be inevitably non-ideal fluctuation in the oscillation behavior, causing the accuracy degradation of networks. In this paper, we investigate the Mott neuronal oscillation fluctuation (NOF) through experiments and modeling. The results show that the NOF phenomenon conforms to Gaussian distribution and originates from thermal fluctuation induced switching voltage variations. We construct a two-layer CSNN for image recognition tasks to study the NOF effect and propose the activation function boundary (AFB) method to strengthen the stability of the network. The results indicate that AFB can improve the accuracy of CSNN by up to 15.5% by tightening output distribution.

Keywords Mott neuron, oscillation fluctuation, variation-aware Mott neuronal model, conversion-based spiking neural network, activation function boundary

1 Introduction

Neuromorphic computing, inspired by the human brain, has drawn great attention owing to the potential of breaking the Von-Neumann bottleneck [1–3]. Particularly, the spiking neural network (SNN) composed of neurons and synapses has been developing rapidly owing to the advantage of high energy efficiency compared with traditional deep-learning networks (DLNs) [4,5]. However, SNN suffers from low inference accuracy [6]. To solve this problem, the conversion-based spiking neural network (CSNN) was proposed. CSNN possesses both remarkable energy efficiency, inheriting from SNN, and high accuracy, inheriting from the neuronal behaviors matching with activation functions of DLNs [7,8].

In CSNN, the neuron is a basic element and plays a vital role in achieving high inference accuracy for various tasks. Nowadays, various kinds of neuronal circuits have been implemented [9,10]. Among the neurons, the Mott neuron has shown great potential due to its simple structure and low power consumption [11,12]. The typical Mott neuron is composed of a Mott device in series with a tunable load resistor (TLR). The Mott device, such as the VO_2-based device, exhibits stable threshold switching behaviors and great endurance characteristics, which is the foundation of Mott neuronal oscillation behavior [13–15]. The firing rates are modulated by tuning the TLR conductance to emulate the rectified linear unit (ReLU) function in CSNN [16,17]. Based on Mott neurons, the CSNN has been demonstrated in the RRAM-based hardware platform, showing great energy efficiency and low hardware cost [18]. However, recent reports indicate that the oscillation behavior of Mott neurons exhibits non-ideal fluctuation, leading to

* Corresponding author (email: wangzongwei@pku.edu.cn, caiyimao@pku.edu.cn)
† Wu L D and Wang Z W have the same contribution to this work.

a mismatch between neuronal output response and ReLU function [19]. Consequently, the accuracy of networks will be affected.

In this work, we investigate the Mott neuronal oscillation fluctuation (NOF) phenomenon experimentally based on the TiN/VO_2/TaO_x/Pt device. The results indicate that the mean interval (T_i) of neuronal firing spikes conforms to the Gaussian distribution. We further develop a variation-aware neuronal oscillation model to capture the relationship between the NOF phenomenon and switching voltage variations that originate from thermal fluctuation in the local VO_2 conductive path. Finally, we construct a two-layer CSNN to examine the NOF effect on inference accuracy for image recognition tasks. The results indicate that NOF can reduce inference accuracy by 24.8%. By introducing the proper activation function boundary (AFB), the output distribution can be effectively tightened. The accuracy of CSNN can be improved by up to 15.5%. This work provides guidelines for the construction of Mott-based CSNNs with high reliability.

2 Experiments

The Mott device is composed of a structure of TiN/VO_2/TaO_x/Pt as shown in Figure 1(a) inset. A detailed fabrication process can be found in [20, 21]. The electrical characteristics of the Mott device and the oscillation behavior of the Mott neuron were measured by an Agilent B1500A semiconductor parameter analyzer. The oscillatory waveforms of the neuron were captured by a Tektronix MSO 2024B oscilloscope. The simulation of the variation-aware neuronal oscillation model and image recognition tasks of CSNN were carried out by MATLAB.

3 Results and discussions

3.1 VO_2-based device characteristic

For the stacked Mott device (Figure 1(a) inset), the VO_2 layer exhibits threshold switching characteristics and the resistance of the TaO_x layer can be adjusted to modulate the switching voltages of the device [20]. When the TaO_x layer is in the low resistance state (LRS), the device shows stable threshold switching behaviors for 100 cycles under dc mode with a 100 μA compliance current (I_{cc}), as shown in Figure 1(a). During electrical measurement, the voltage is applied to the TiN electrode, and the Pt electrode is always kept grounded. As can be seen, the current increases drastically when the applied voltage increases above 0.76 V (V_{th} = 0.76 V) during the forward sweep. During backward sweep, the current abruptly decreases when the voltage is below 0.36 V (V_{hold} = 0.36 V). Figure 1(b) shows the switching mechanism of the Mott device when the TaO_x layer is in LRS. The threshold switching behavior originated from the formation and annihilation of the local conductive path in the VO_2 layer, which is caused by the heat-induced regional phase change [21]. Figure 1(c) exhibits cycle-to-cycle uniformity of the high resistance state (HRS) and LRS of the Mott device for 100 cycles. The on/off ratio is always larger than 10. Figure 1(d) shows the HRS and LRS of 10 devices under the same operating condition.

3.2 Mott NOF

Based on the repeatable threshold switching characteristic, the neuronal oscillation behavior can be achieved by a simple circuit structure composed of the Mott device and a TLR in series, as shown in Figure 2(a). When an input stimulus (V_{in}) is applied to the circuit, the voltage (V_{out}) exhibits oscillatory waveforms due to the charging and discharging process of inherent parasitic capacitance (C_i) of the Mott device. Figure 2(b) shows the typical oscillation behavior with 83.3 kHz frequency when V_{in} is 4 V and the resistance of TLR (R_L) is 50 kΩ. As can be seen from Figure 2(b), the T_i of neuronal firing spikes varies between adjacent spikes ($T_{i1} \neq T_{i2}$), which confirms the existence of the NOF phenomenon in Mott neurons.

We systematically study the NOF phenomenon based on the Mott neuronal circuit by fixing V_{in} to 4 V and varying R_L. T_i is the mean interval of neuronal firing spikes and the distribution of T_i can be used to characterize the NOF phenomenon. We define the number of neuronal continuous firing spikes as N_{spike}, which could be used to characterize the monitoring time of the system. Here, we select a group of N_{spike}s to calculate the T_is based on experimental neuronal oscillation behaviors. Figure 3 shows the statistical results of T_i under different N_{spike}s. The NOF phenomenon always exists regardless of

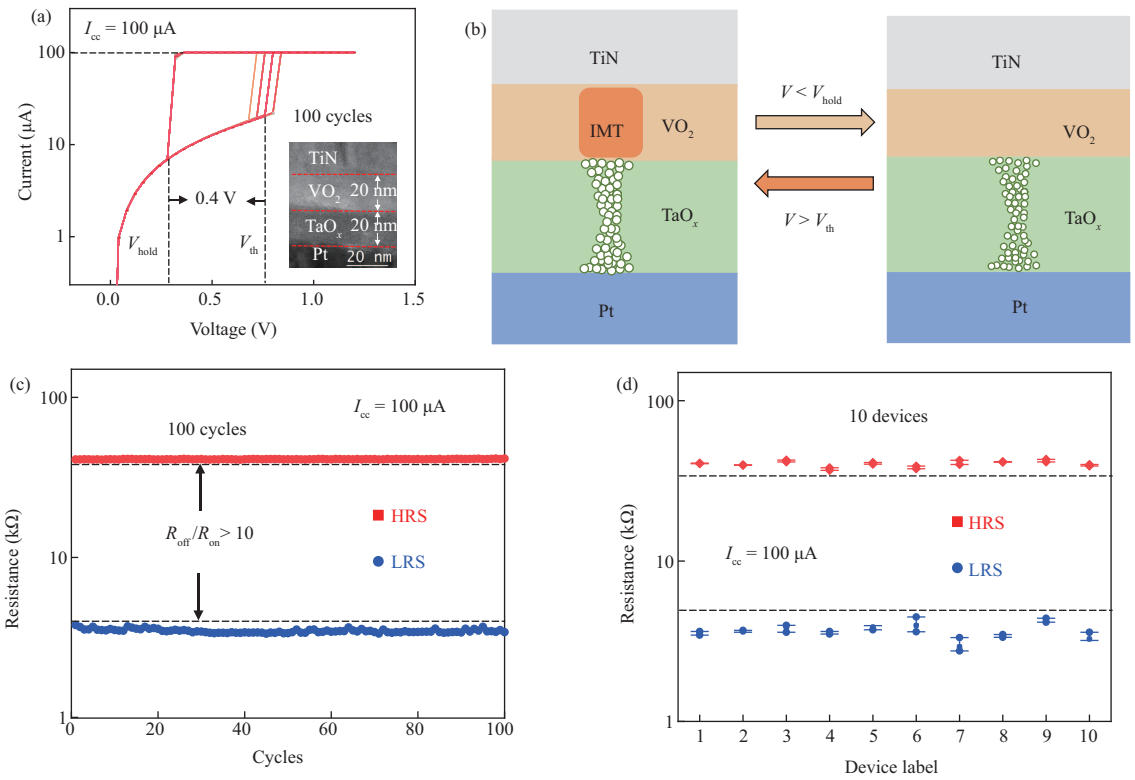

Figure 1 (Color online) (a) Threshold switching characteristic of the device for 100 cycles under 100 μA compliance current. Inset: device structure of transmission electron microscope (TEM). (b) Schematic mechanism of threshold switching behavior of the Mott device when the TaO_x layer is in LRS. (c) Cycle-to-cycle uniformity of the device for 100 cycles when I_{cc} = 100 μA. (d) Device-to-device uniformity of 10 devices under the same operating condition.

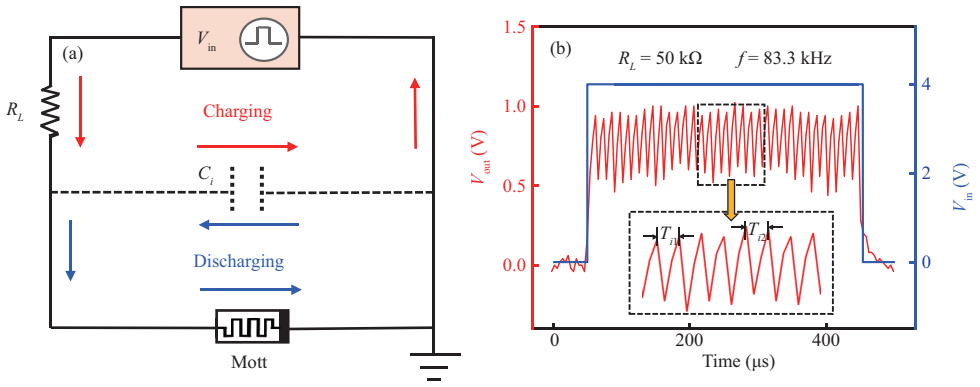

Figure 2 (Color online) (a) Schematic circuit structure of the Mott neuron. C_i is the inherent parasitic capacitance of the Mott device. (b) Typical oscillation behavior of the Mott neuron when V_{in} is 4 V and R_L is 50 kΩ.

how R_L and N_{spike} change. Moreover, with the increase of R_L, the distribution of T_i shows a redshift, indicating an increase in neuronal firing spike interval. Figure 4(a) shows the Gaussian fitting result of the measured NOF phenomenon. The mean value (μ_t) extracted from experimental T_i distribution is 12 μs. The extracted standard deviation ($\sigma_t = 1.97\times10^{-6}$) shows the strength of the NOF phenomenon. As can be seen from Figure 4(b), μ_t increases with R_L increasing, but is irrelevant to N_{spike}. Figure 4(c) shows that σ_t decreases with R_L decreasing or N_{spike} increasing, indicating that extending monitoring time can alleviate the NOF phenomenon. However, this will inevitably introduce extra latency to the system.

The charging and discharging processes of the Mott neuron are related to HRS, LRS, threshold voltage (V_{th}) and hold voltage (V_{hold}). Therefore, we statistically analyzed the distribution of HRS, LRS, V_{th}, and V_{hold}. Figure 5(a) indicates stable switching behaviors of the device for 1000 cycles. The trend of HRS and LRS is shown in Figure 5(b), indicating only slight cycle-to-cycle fluctuations, which has little effect

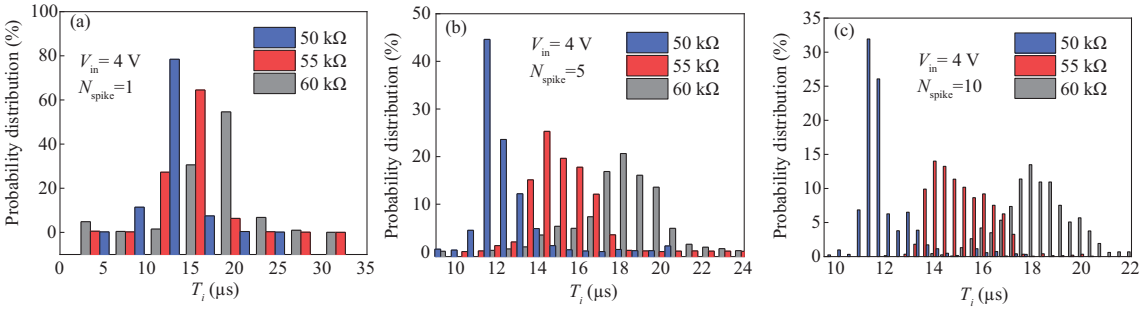

Figure 3 (Color online) Distributions of T_i of neuronal firing spikes when varying R_L (R_L = 50, 55, and 60 kΩ, respectively) and considering different N_{spike}s. (a) N_{spike} = 1; (b) N_{spike} = 5; (c) N_{spike} = 10.

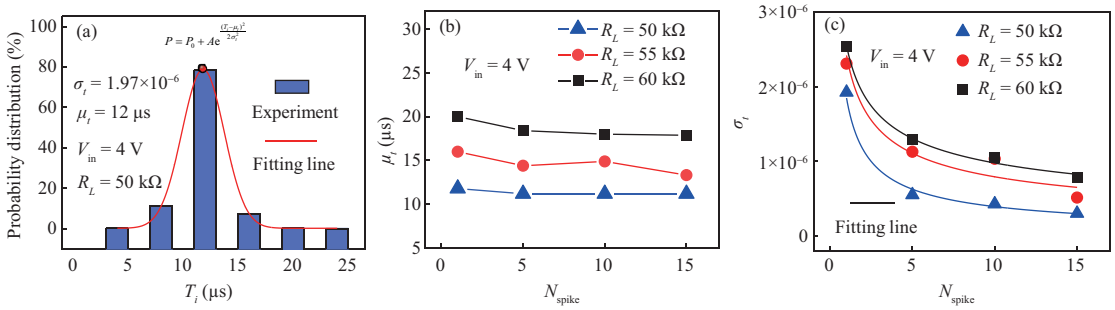

Figure 4 (Color online) (a) Fitting result of T_i distribution when V_{in} is 4 V and R_L is 50 kΩ. Trend of (b) extracted mean value (μ_t) and (c) standard deviation (σ_t) when R_L and N_{spike} are adjusted. μ_t increases with R_L increasing, but is irrelevant to N_{spike}. σ_t decreases with R_L decreasing or N_{spike} increasing.

on neuronal charging and discharging processes. Figure 5(c) shows the distribution of V_{th}, which accords with the Gaussian distribution. The extracted mean V_{th} (μ_V) and standard deviation (σ_V) are 0.84 V and 0.02008, respectively. Figure 5(d) shows the fluctuation of V_{hold}. According to the insulator-metal-transition (IMT) mechanism and Newton's cooling law [22–24], the threshold switching behavior of Mott devices is related to the Joule heat induced generation and annihilation of the conductive path. Figure 6 shows the generation and dissipation of heat in different stages of the threshold switching behavior. There are four key stages in the switching process when a voltage is applied to the device [25–27]. During forward sweep, when the voltage increases gradually and reaches V_{th} (from stages (1) to (2)), the Joule heat is generated and accumulated. Then the conductive path is generated and the current increases abruptly (stage (3)). However, there are inevitable random thermal fluctuations during the process from stages (1) to (3). Therefore, the conductive path is generated randomly in each transition of the device from HRS to LRS, contributing to the obvious variation of V_{th}. During the backward sweep, the rate of heat dissipation gradually exceeds that of heat generation. When the voltage decreases to V_{hold} (stage (4)), the thermal effect cannot support phase transition, and the device switches from LRS to HRS automatically. During this process, the heat dissipates along the electrodes. Therefore, V_{hold} shows slight fluctuation. The variations of V_{th} and V_{hold} play a vital role in interfering with the charging and discharging time of the Mott neuron, consequently causing the NOF phenomenon.

To demonstrate the relationship between the NOF phenomenon and switching voltage (V_{th} and V_{hold}) variations, we construct a variation-aware Mott neuronal oscillation model based on the charging and discharging processes of Mott neurons. The charging and discharging processes can be expressed by (1)–(4), respectively.

$$V = V_{\text{in}} \times \frac{R_h}{(R_h + R_L)}, \tag{1}$$

$$V_{t+1} = (V - V_t) \times \left(1 - \mathrm{e}^{-\frac{t_0}{\tau}}\right) + V_t, \tag{2}$$

$$V = V_{\text{in}} \times \frac{R_l}{(R_l + R_L)}, \tag{3}$$

$$V_{t+1} = V_t \times \mathrm{e}^{-\frac{t_0}{\tau}}, \tag{4}$$

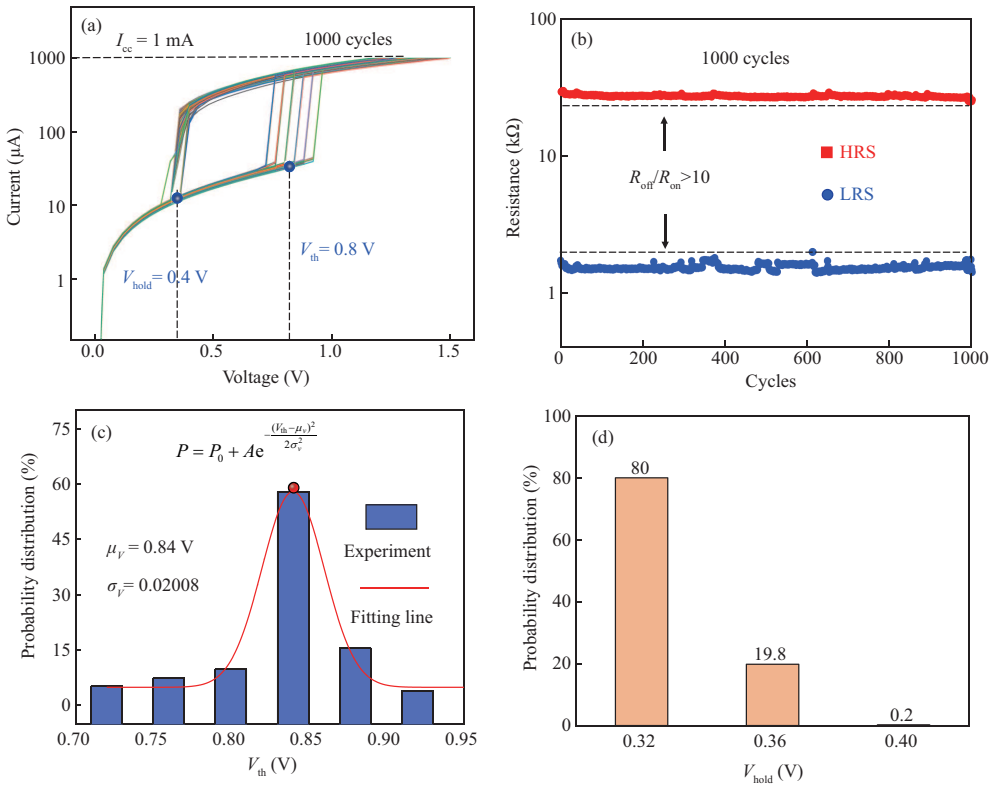

Figure 5 (Color online) (a) Repeatable threshold switching characteristics of the device for 1000 cycles when I_{cc} is 1 mA; (b) the endurance characteristic of the device; (c) the distribution and fitting result of V_{th}; (d) the distribution of V_{hold}.

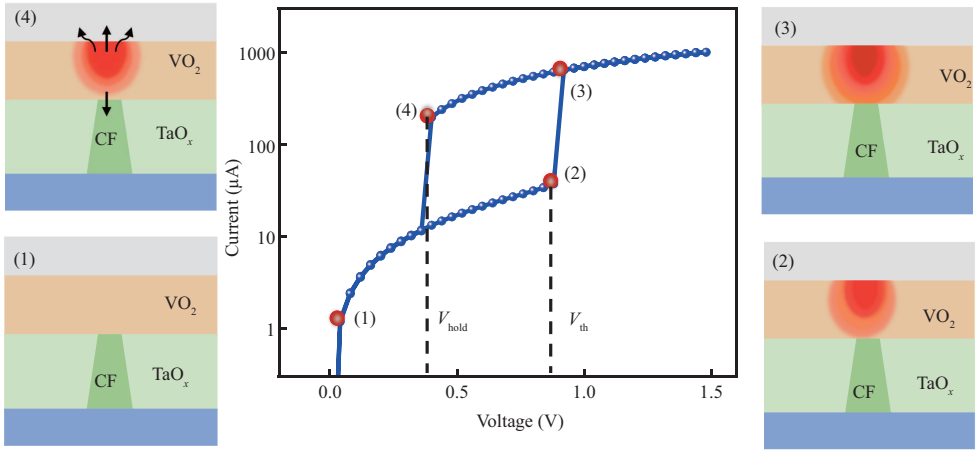

Figure 6 (Color online) Schematic of the generation and dissipation of heat in different stages of the threshold switching behavior.

where R_h and R_l are high and low resistance of the Mott device respectively. t_0 is the unit time. τ is the time constant of C_i and V_t is the voltage on the device at time t. Figure 7 shows the procedure of neuronal oscillation simulation. According to experimental results, the relevant parameters adopted in the model are shown in Table 1. Figure 8 shows simulation results when switching voltage variations are ignored. The simulated neuron exhibits stable and consistent oscillation behaviors. Moreover, the oscillation frequency decreases with the increase of R_L, which is consistent with experimental results. We further introduce switching voltage noises (Θ_{th} and Θ_{hold}) in the model. According to the above extracted results, we set V_{th} to Gaussian distribution with the mean value of 0.8 V and standard deviation of 0.02 and add a slight disturbance to V_{hold}. Figure 9(a) shows the simulated and experimental neuronal oscillation behaviors when V_{in} is 4 V and R_L is 50 kΩ. The fitting result indicates that simulated neuronal μ_t is also 12 μs and σ_t is close to that of experimental results (Figure 9(b)), demonstrating that switching voltage

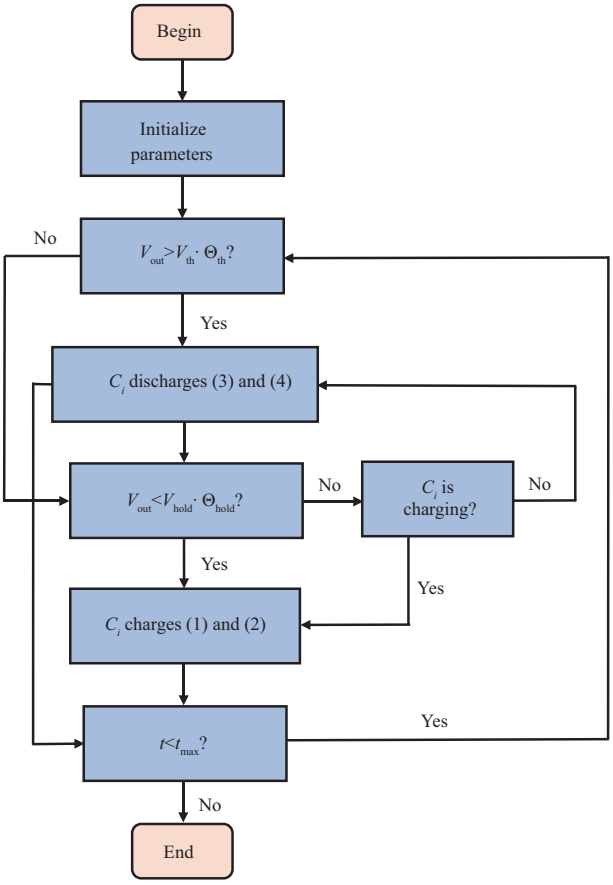

Figure 7 (Color online) Flow chart of the variation-aware Mott neuronal oscillation model we constructed. $\Theta_{\rm th}$ and $\Theta_{\rm hold}$ are noises applied on $V_{\rm th}$ and $V_{\rm hold}$, repectively.

Table 1 Parameters adopted in the variation-aware Mott neuronal oscillation model

$V_{\rm th}$	$V_{\rm hold}$	R_h	R_l	$V_{\rm in}$	τ
0.8 V	0.4 V	40 kΩ	3 kΩ	4 V	12 μs

variations contribute to the NOF phenomenon.

3.3 Effect and mitigation of NOF

Finally, a two-layer CSNN for the MNIST (Mixed National Institute of Standards and Technology database) recognition task is constructed to investigate the NOF effect, as shown in Figure 10. There are 784 input neurons and 10 output neurons in the network. The hidden layer consists of 50 neurons. The neuron is formed by serially connecting the Mott device with the source of MOSFET. The pre-layer output is input in the gate of MOSFET to regulate the resistance of the transistor and a fixed voltage ($V_{\rm DD}$) is applied to the neuron. The Mott neuronal oscillation frequency is converted into a voltage signal by peripheral circuits and then transferred to the next layer. The neuron with the highest oscillation frequency in the output layer represents the recognition result. Figure 11(a) shows the training and inference accuracy against training cycles. To study the NOF effect, it is necessary to quantify neuronal outputs. During 50 inference processes, the outputs of CSNN are always smaller than 5, as shown in Figure 11(b). Therefore, we define the maximum output of neurons as 5 when quantizing neuronal output. According to experimental results, we set NOF with σ_t of 3×10^{-6} as the maximum noise and introduce noises in CSNN by matching NOF with output. The way of applying NOF noise is expressed as follows:

$$f_{\rm ideal} = \frac{x}{2^n} \times (f_h - f_l) + f_l, \tag{5}$$

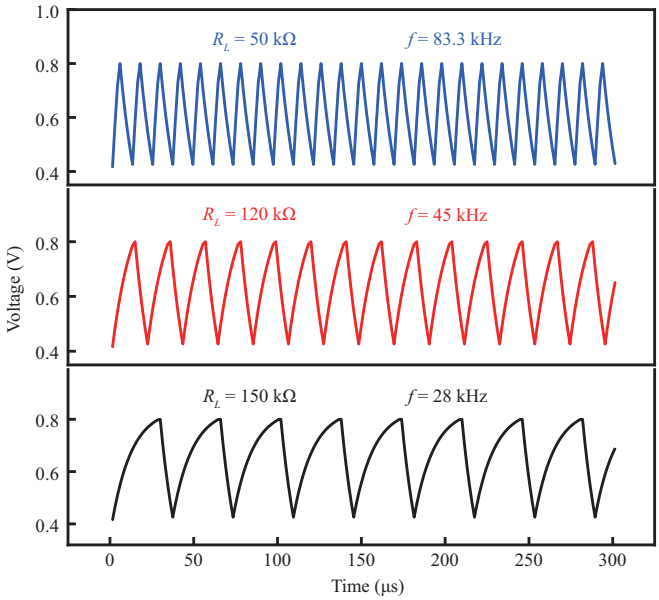

Figure 8 (Color online) Simulated neuronal oscillation behaviors based on the variation-aware Mott neuronal oscillation model when R_L changes (R_L = 50, 120, and 150 kΩ, respectively) and switching voltage noises are ignored.

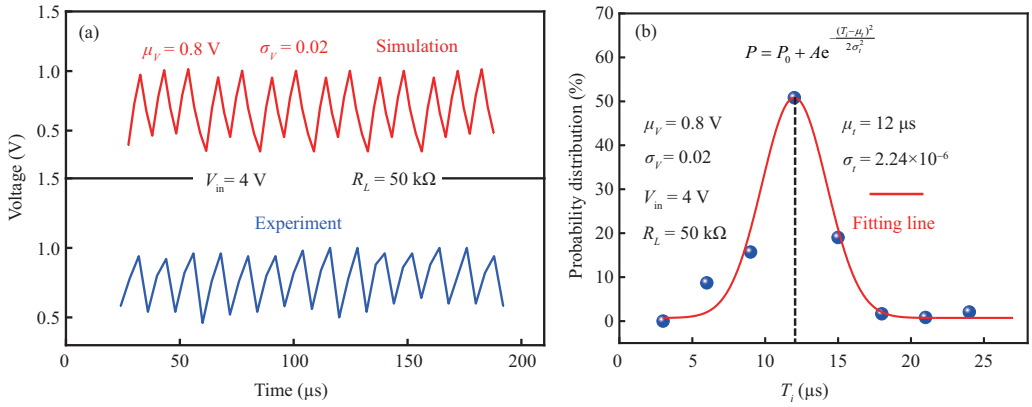

Figure 9 (Color online) (a) Oscillation behaviors of simulated and experimental neurons when switching voltage noises are introduced; (b) fitting result of simulated neuronal T_i distribution when switching voltage noises are considered.

$$t_1 = \frac{1}{f_{\text{ideal}}} + G(\sigma_t), \tag{6}$$

$$y = \frac{\frac{1}{t_1} - f_l}{f_h - f_l} \times 2^n, \tag{7}$$

where x is the input to the Mott neuron and n is the quantization precision. The f_h and f_l are the highest and lowest neuronal oscillation frequency respectively. The f_{ideal} is the ideal output frequency of the neuron. $G(\sigma_t)$ is the NOF noise with a strength of σ_t. y is the final output of the neuron when NOF noise is considered. Figure 11(c) shows inference accuracy against NOF noise strength (σ_t) when different output bits are considered. As can be seen, when the quantization accuracy of the Mott neuron is 2 bits, the inference accuracy decreases by up to 24.8%. What is worse, the accuracy drops 5.43% even when a 6-bit neuron is adopted, which poses a great challenge to Mott device performance and thus needs to be solved.

To mitigate the influence of NOF noise, we propose the AFB method that can confine the output of

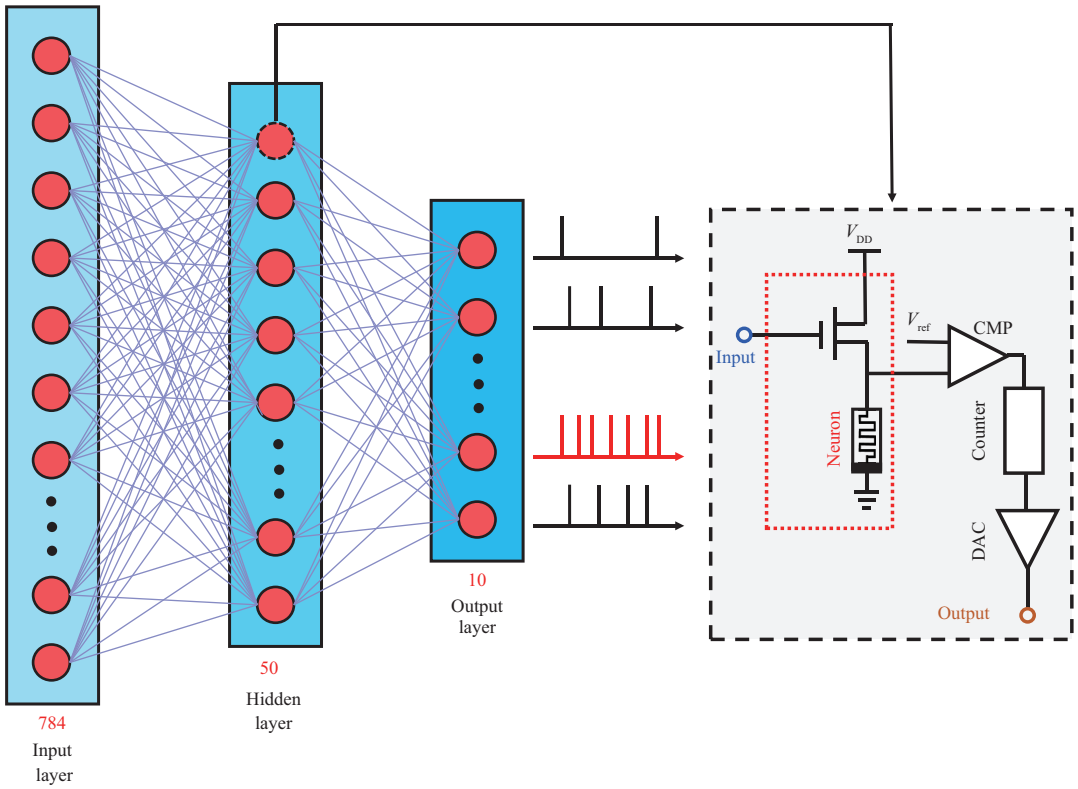

Figure 10 (Color online) Schematic of the constructed two-layer conversion-based SNN.

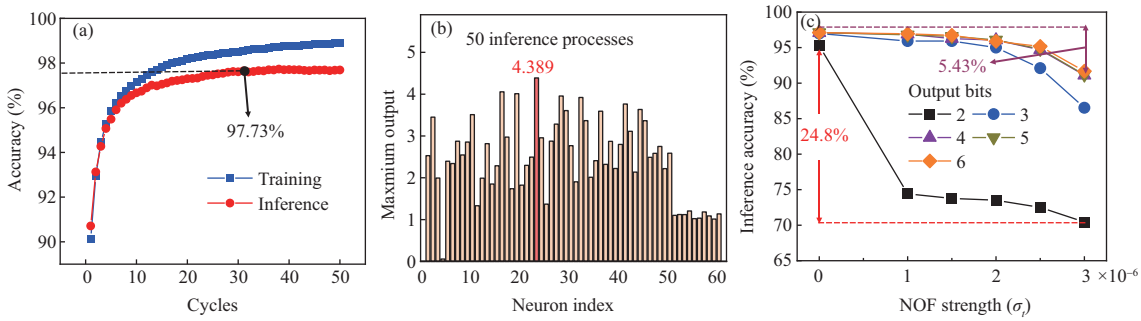

Figure 11 (Color online) (a) Training and inference accuracy against training cycles of the network; (b) maximum outputs of neurons in CSNN for 50 inference processes; (c) accuracy against NOF noise strength (σ_t) and output bits.

neurons in an appropriate range (inset in Figure 12). The AFB method can be expressed as follows:

$$f(x) = \begin{cases} 0, & x < 0, \\ x, & 0 \leqslant x < b, \\ b, & b \leqslant x, \end{cases} \tag{8}$$

where x is the input to the Mott neuron and b is the boundary we set. Based on the AFB method, regardless of the value input to the neuron, the output of the neuron is always no greater than b. Figure 12 shows the inference accuracy against the output boundary. When the boundary is 1.5, the accuracy is 97.1%, which is close to that of the network without a boundary. Therefore, we set the boundary to 1.5 and construct two CSNNs to demonstrate the effect of the AFB method. One of the networks adopts the AFB method and the other one has no output boundary. Figure 13 shows the comparison of inference accuracy of these two networks when NOF noises are considered. As can be seen, the AFB method can effectively strengthen the robustness of CSNN and promote accuracy by up to 15.5% when a 2-bit neuron is adopted. Figure 14(a) shows the outputs of the hidden layer of the network without a boundary for 50

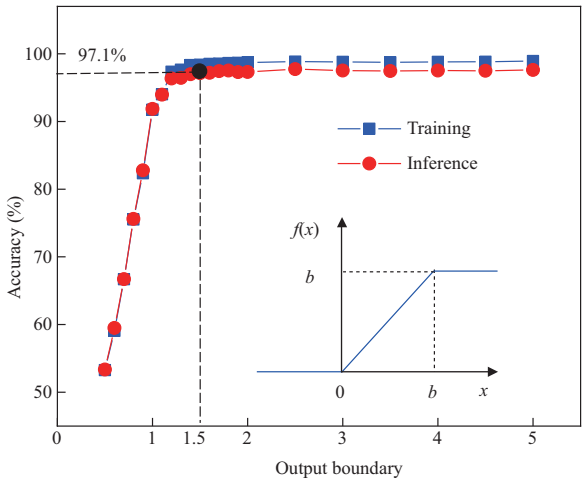

Figure 12 (Color online) Training and inference accuracy of CSNN against output boundary. Inset: schematic of our proposed AFB method.

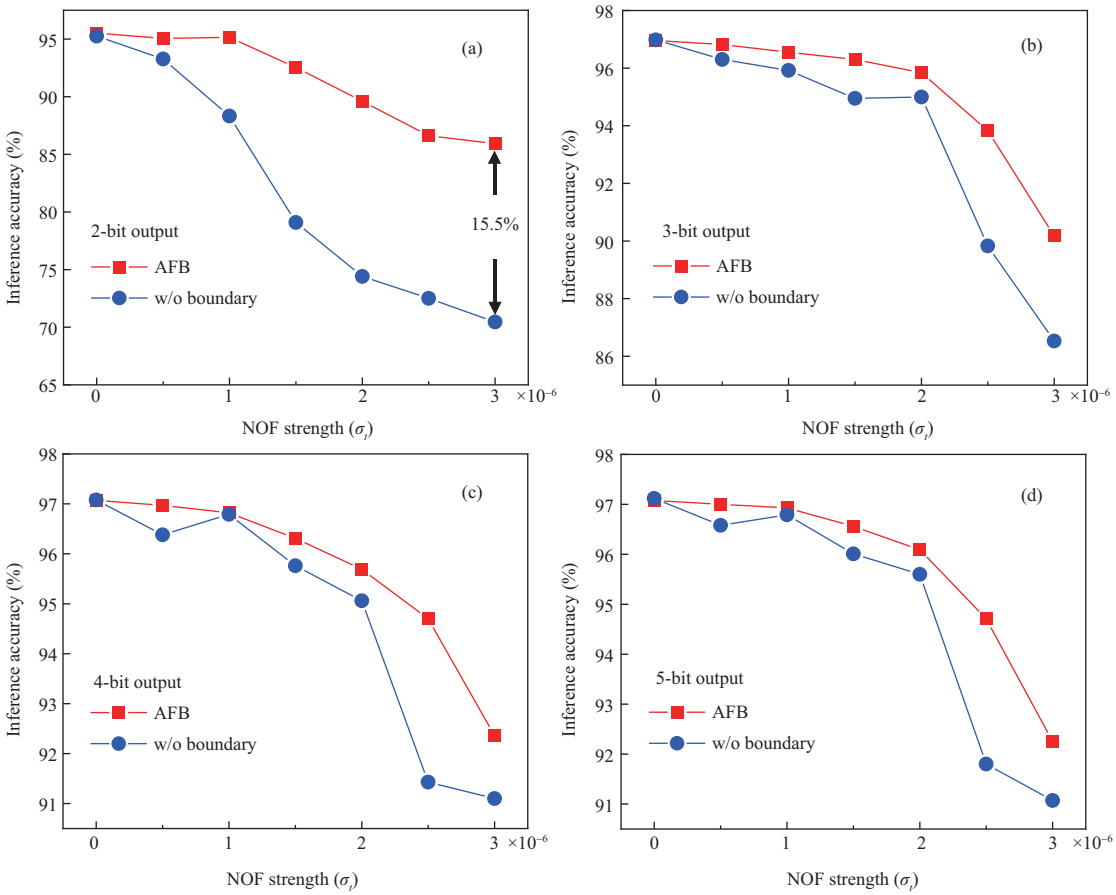

Figure 13 (Color online) Comparisons of inference accuracy of the two CSNNs when NOF noises (σ_t) and different output bits are adopted. The quantization precision of neuronal output is (a) 2 bits, (b) 3 bits, (c) 4 bits, and (d) 5 bits, respectively.

inference processes before and after NOF noise of 1×10^{-6} is applied. Figure 14(b) indicates those of the network adopting the AFB method. Table 2 shows characteristic values of output difference of these two networks before and after applying NOF noises. These results indicate that the AFB method can keep the system more stable by tightening output distribution.

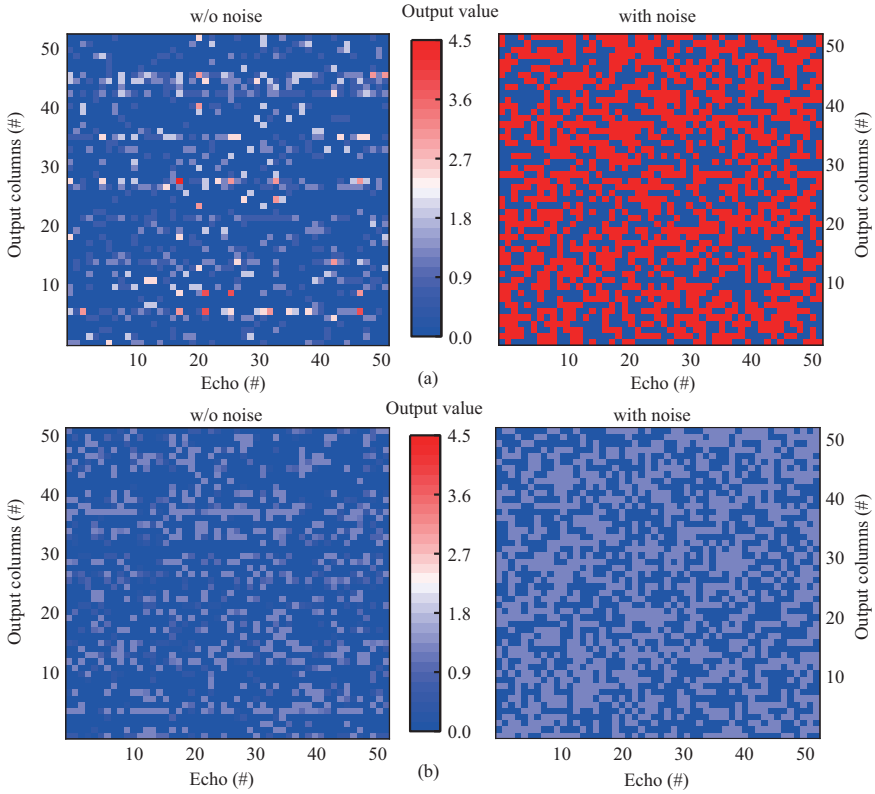

Figure 14 (Color online) Outputs of CSNNs ((a) without boundary and (b) adopting AFB method) before and after NOF noise of 1×10^{-6} is considered for 50 inference processes.

Table 2 Characteristic values of output difference of two networks before and after applying NOF noises

	Mean	Maximum	Minimum
w/o boundary	1.9615	4.375	−3.75
AFB	**0.3253**	**1.3125**	**−1.3125**

4 Conclusion

In this work, we investigate the NOF phenomenon based on the Mott device for the first time. Experimental results show that the NOF phenomenon accords with Gaussian distribution. We further construct a variation-aware Mott neuronal oscillation model to demonstrate the relationship between the NOF phenomenon and switching voltage variations induced by thermal fluctuation. The simulation results based on a two-layer CSNN for image recognition task indicate that NOF can reduce inference accuracy by up to 24.8% due to the mismatch between neuronal output and ReLU function. Finally, we propose the AFB method to enhance the robustness of CSNN and improve inference accuracy by 15.5% at most by tightening output distribution. This work provides guidelines for constructing stable and high-precision SNN systems based on Mott neurons.

Acknowledgements This work was supported by National Key R&D Program of China (Grant No. 2019YFB2205401), National Natural Science Foundation of China (Grant Nos. 61834001, 62025401, 61927901), Beijing Nova Program (Grant No. 20220484113), and 111 project (Grant No. B10081).

References

1 Zhang Z H, Wang Z W, Shi T, et al. Memory materials and devices: from concept to application. InfoMat, 2020, 2: 261–290
2 Wu L D, Wang Z W, Wang B W, et al. Emulation of biphasic plasticity in retinal electrical synapses for light-adaptive pattern pre-processing. Nanoscale, 2021, 13: 3483–3492
3 Zhao Y L, Yang J L, Li B, et al. NAND-SPIN-based processing-in-MRAM architecture for convolutional neural network acceleration. Sci China Inf Sci, 2023, 66: 142401
4 Han Y N, Xiang S Y, Zhang T R, et al. Conversion of a single-layer ANN to photonic SNN for pattern recognition. Sci China Inf Sci, 2024, 67: 112403
5 Pei J, Deng L, Ma C, et al. Multi-grained system integration for hybrid-paradigm brain-inspired computing. Sci China Inf Sci, 2023, 66: 142403

6 Roy K, Jaiswal A, Panda P. Towards spike-based machine intelligence with neuromorphic computing. Nature, 2019, 575: 607–617
7 Sengupta A, Ye Y T, Wang R, et al. Going deeper in spiking neural networks: VGG and residual architectures. Front Neurosci, 2019, 13: 95
8 Zhang X M, Wang Z R, Song W H, et al. Experimental demonstration of conversion-based SNNs with 1T1R Mott neurons for neuromorphic inference. In: Proceedings of IEEE International Electron Devices Meeting, San Francisco, 2019
9 Wang Z R, Rao M Y, Han J W, et al. Capacitive neural network with neuro-transistors. Nat Commun, 2018, 9: 3208
10 Bao L, Kang J, Fang Y C, et al. Artificial shape perception retina network based on tunable memristive neurons. Sci Rep, 2018, 8: 13727
11 Wu L D, Wang Z W, Bao L, et al. Implementation of neuronal intrinsic plasticity by oscillatory device in spiking neural network. IEEE Trans Electron Dev, 2022, 69: 1830–1834
12 Fu Y Y, Zhou Y, Huang X, et al. Forming-free and annealing-free V/VO_x/$HfWO_x$/Pt device exhibiting reconfigurable threshold and resistive switching with high speed (<30 ns) and high endurance (>10^{12}/>10^{10}). In: Proceedings of IEEE International Electron Devices Meeting, San Francisco, 2021
13 Yan B N, Yang Y C, Huang R. Memristive dynamics enabled neuromorphic computing systems. Sci China Inf Sci, 2023, 66: 200401
14 Lee D, Kwak M, Moon K, et al. Various threshold switching devices for integrate and fire neuron applications. Adv Elect Mater, 2019, 5: 1800866
15 Zhang X M, Zhuo Y, Luo Q, et al. An artificial spiking afferent nerve based on Mott memristors for neurorobotics. Nat Commun, 2020, 11: 51
16 Woo J Y, Wang P N, Yu S M. Integrated crossbar array with resistive synapses and oscillation neurons. IEEE Electron Dev Lett, 2019, 40: 1313–1316
17 Duan Q X, Jing Z K, Zou X L, et al. Spiking neurons with spatiotemporal dynamics and gain modulation for monolithically integrated memristive neural networks. Nat Commun, 2020, 11: 3399
18 Zhang X M, Wu Z, Lu J K, et al. Fully memristive SNNs with temporal coding for fast and low-power edge computing. In: Proceedings of IEEE International Electron Devices Meeting, San Francisco, 2021
19 Kim G M, In J H, Kim Y S, et al. Self-clocking fast and variation tolerant true random number generator based on a stochastic Mott memristor. Nat Commun, 2021, 12: 2906
20 Wang Z W, Zheng Q L, Kang J, et al. Self-activation neural network based on self-selective memory device with rectified multilevel states. IEEE Trans Electron Dev, 2020, 67: 4166–4171
21 Bao L, Wang Z W, Wang B W, et al. Tunable stochastic oscillator based on hybrid VO_2/TaO_x device for compressed sensing. IEEE Electron Dev Lett, 2020, 42: 102–105
22 Pickett M D, Stanley Williams R. Sub-100 fJ and sub-nanosecond thermally driven threshold switching in niobium oxide crosspoint nanodevices. Nanotechnology, 2012, 23: 215202
23 Kumar S, Strachan J P, Williams R S. Chaotic dynamics in nanoscale NbO_2 Mott memristors for analogue computing. Nature, 2017, 548: 318–321
24 Kumar S, Wang Z W, Davila N, et al. Physical origins of current and temperature controlled negative differential resistances in NbO_2. Nat Commun, 2017, 8: 658
25 Yuan R, Duan Q, Tiw P J, et al. A calibratable sensory neuron based on epitaxial VO_2 for spike-based neuromorphic multisensory system. Nat Commun, 2022, 13: 3973
26 Shao Z W, Cao X, Luo H J, et al. Recent progress in the phase-transition mechanism and modulation of vanadium dioxide materials. NPG Asia Mater, 2018, 10: 581–605
27 Schofield P, Bradicich A, Gurrola R M, et al. Harnessing the metal-insulator transition of VO_2 in neuromorphic computing. Adv Mater, 2023, 35: 2205294